THE JOURNAL OF PHYSICAL CHEMISTRY A

pubs.acs.org/JPCA Article

Optimizing the Energetics of FLP-Type H_2 Activation by Modulating the Electronic and Structural Properties of the Lewis Acids: A DFT Study

Mojgan Heshmat* and Bernd Ensing

Cite This: J. Phys. Chem. A 2020, 124, 6399−6410 Read Online

ACCESS | Metrics & More | Article Recommendations | Supporting Information

ABSTRACT: The great potential of frustrated Lewis pairs (FLPs) as metal-free catalysts for activation of molecular hydrogen has attracted increasing interest as an alternative to transition-metal catalysts. However, the complexity of FLP systems, involving the simultaneous interaction of three molecules, impedes a detailed understanding of the activation mechanism and the individual roles of the Lewis acid (LA) and Lewis base (LB). In the present work, using density functional theory (DFT) calculations, we examine the reactivity of 75 FLPs for the H_2 splitting reaction, including a series of experimentally investigated LAs combined with conventional phosphine-based (tBu_3P) and oxygen-based (i.e., ethereal solvent) Lewis bases. We find that the catalytic activity of the FLP is the result of a delicate balance of the LA and LB strengths and their bulkiness. The H_2 splitting reaction can be changed from endergonic to exergonic by tuning the electrophilicity of the LA. Also, a more nucleophilic LB results in a more stable ion pair product and a lower barrier for the hydrogen splitting. The bulkiness of the LB leads to an early transition state to reduce steric hindrance and lower the barrier height. The bulkiness of the fragments determines the cavity size in the FLP complex, and a large cavity allows for a larger charge separation in the ion pair configuration. A shorter proton−hydride distance in this product complex correlates with a stronger attraction between the fragments, which forms more reactive ion pairs and facilitates the proton and hydride donations in the subsequent hydrogenation process. These insights may help with rationalizing the experimentally observed reactivities of FLPs and with designing better FLP systems for hydrogenation catalysis and hydrogen storage.

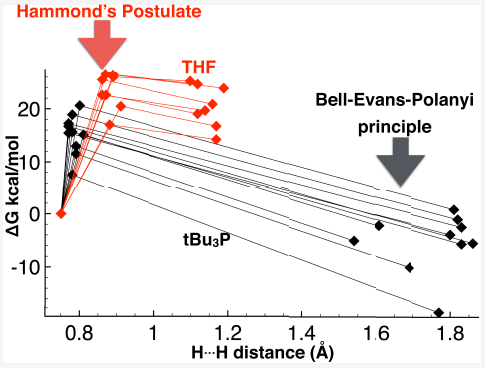

1. INTRODUCTION

The H_2 molecule is an essential component in various chemical processes. It has a promising role as a clean energy source, and it supplies hydrogen atoms in hydrogenation reactions. Activation of the molecule hydrogen is therefore an important research topic in catalysis.[1,2] Since the H_2 molecule has a strong covalent bond and very low polarizability, activation of the hydrogen molecule remains a difficult task.

Catalytic H_2 activation hinges on the use of transition metals, taking advantage of the catalytic properties of these d-block elements.[3] While transition-metal catalysis remains indisputably important in many fields of chemistry, the advent of the metal-free frustrated Lewis pair (FLP) concept for activation of small molecules, such as H_2, and FLP-catalyzed hydrogenation reactions has attracted increasing interest ever since Stephan et al. reported their pioneering metal-free reversible H_2 activation in 2006.[4]

The fundamental notion underlying FLP chemistry is that a bulky Lewis acid (LA) and a bulky Lewis base (LB) do not quench into the usual Lewis adduct. For example, the now prototypical $B(C_6F_5)_3/P(tBu)_3$ pair and its analogues have sufficient steric hindrance to prevent the LB−LA dative bond formation.[5,6] In addition to sterically hindered FLPs, there are also thermally induced FLPs, in which the LA and LB are in equilibrium with their corresponding Lewis adduct at high enough temperatures.[7−9] The application of FLP chemistry has been expanded and, during the past decade, developed to include a broad range of new reactions and modifications of advanced chemical systems, including heterogeneous and solid-phase FLPs and frustrated radical pairs.[10−16] The mechanistic aspects of FLP systems have been subjected to theoretical investigations. The optimal distance of the LA/LB centers has been determined by modifying the LA and LB structures to increase the reactivity and the efficiency of FLPs. The electronic structures and molecular orbital interactions have been analyzed to rationalize the FLP reactivity, and theoretical models have been applied to a wide range of FLPs to characterize the existing FLP systems and design new ones.[17−30] In addition, the flexibility and dynamical behavior of

Received: April 7, 2020
Revised: July 13, 2020
Published: July 15, 2020

https://dx.doi.org/10.1021/acs.jpca.0c03108
J. Phys. Chem. A 2020, 124, 6399−6410

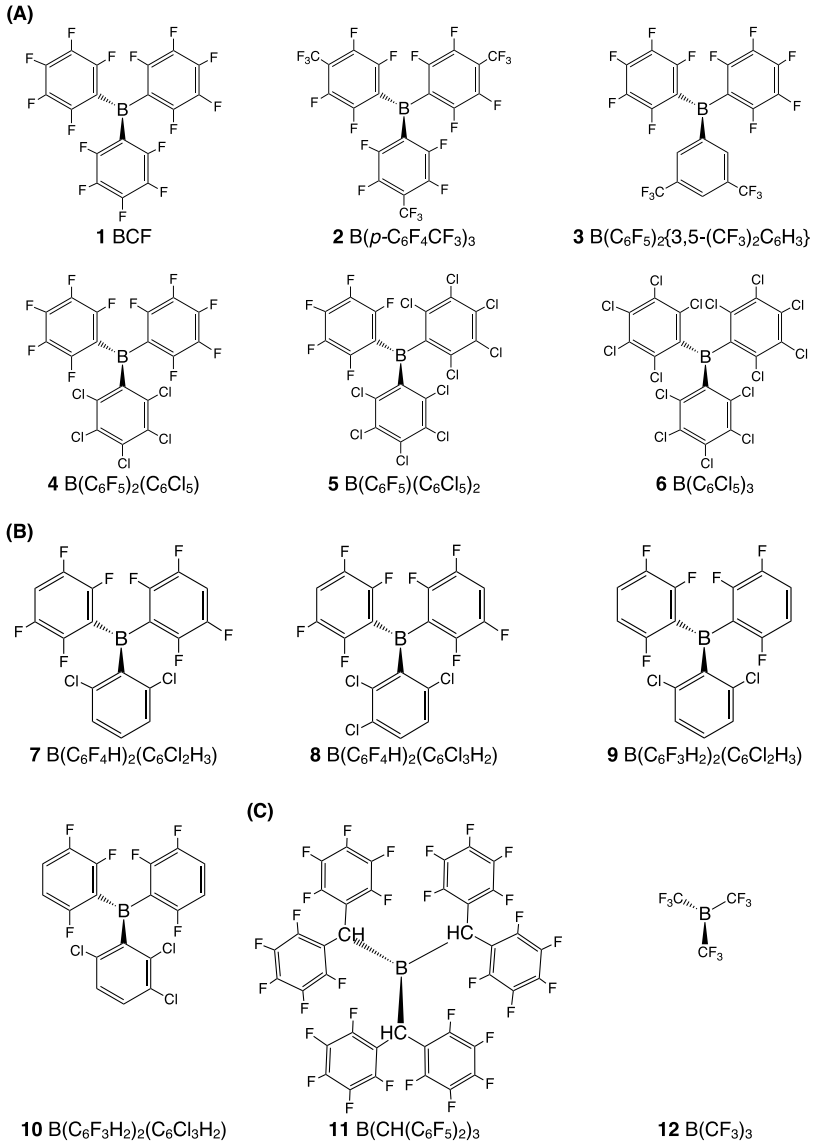

Figure 1. Lewis acids (LAs) considered in this work. Variation of the number of F atoms in the aryl rings or addition of bulkier groups in place of F atoms alters the electronic and structural properties of the BCF derivatives. All of the BCF derivatives have a flat geometry in the free molecule.

FLP systems, including in transition-state (TS) geometries, have been subjected to several molecular dynamics investigations.[31−34]

The crucial point in FLP chemistry is that the LA and LB molecules should possess enough noncovalent interactions to form an encounter complex (transient) to be able to activate hydrogen or other small molecules. Calorimetric and kinetic studies have shown that entropic effects play an essential role in the formation of the complex, containing the Lewis acid, the hydrogen molecule, and the Lewis base, and strongly affect the thermodynamics of the H_2 activation.[35] To enable the rational design and successful synthesis of efficient FLP catalysts, several critical aspects have to be carefully considered, including the materials' choice, interaction manipulation between a Lewis acid and base to form an FLP, the spatial architecture of the interfacial Lewis acidic and basic sites, and the actual Lewis acidity/basicity.

H_2 activation has been extensively studied using various LBs combined with $B(C_6F_5)_3$ (BCF hereafter) as the LA, thereby addressing the association of the LA and LB in the form of Lewis adducts (i.e., through dative bond formation) or van der Waals (VdW) adducts, the interactions at the transition state (TS), and the thermodynamics of the H_2 activation. However, the role of the LA in H_2 activation has not been investigated in much detail. Besides, oxygen-based LBs (ethereal solvents), which show catalytic activity for FLP hydrogenation of carbonyl (C═O) compounds,[7−9,36−39] have not yet been studied theoretically.

In this work, we have selected 12 borane-derived LAs and explored the FLP reactivity toward activation of H_2 in the presence of ethereal (O-based) Lewis bases. For comparison, the well-known P-based LBs tBu_3P and Me_3P have also been included. All LAs have previously been shown to activate H_2 experimentally.[23,36,38,40−43] We have examined, using density functional theory (DFT) calculations with a continuum solvation model, the structure and interaction energy of the initial adduct between the LA and LB and the energies of the TS and the product ion pair. The reaction energy of the hydrogen activation is based on the reaction

https://dx.doi.org/10.1021/acs.jpca.0c03108
J. Phys. Chem. A 2020, 124, 6399−6410

$$LA\cdots LB + H_2 \rightleftharpoons [LA\cdots H\cdots H\cdots LB]^{TS} \rightleftharpoons LA - H^{(-)}\ldots{}^{(+)}H - LB \quad (1)$$

Here, we focus our attention on this first step and therefore do not simulate the entire hydrogenation reaction process, including substrate molecules, because this step is common to all hydrogenation reactions. Second, the H_2 activation is predominantly the rate-determining step in hydrogenation reactions, whereas the proton and hydride transfers from the product ion pair, LA−$H^{(-)}\ldots{}^{(+)}$H−LB (**1**), to the substrates generally either have a small barrier or are entirely barrierless.[19,39,44,45]

The paper is organized as follows. First, we present the formation of the initial adduct between the LA and LB and the energetics and structural factors that affect this complexation. Next, the kinetics of the H_2 activation, the energetics of the TSs, and the electronic and structural effects of the LAs and LBs on the activation barrier are described. In the Roles of the Lewis Acid and Base in the Thermodynamics of H_2 Activation section, we explore the thermodynamics of the H_2 activation and the stability of the product ion pair, LA−$H^{(-)}\ldots{}^{(+)}$H−LB. The role of the LAs in the thermodynamics of the reaction will be discussed in the Optimizing the Energetics of H_2 Activation section. In the Conclusions section, we summarize our findings and present a general conclusion about the role of the electronic and structural properties of the LA in the energetics of nonmetal FLP catalytic H_2 activation.

2. COMPUTATIONAL DETAILS

The H_2 activation path for each FLP system was mapped with the linear transit (LT) method using an appropriately chosen reaction coordinate. All LT mappings were started from and ended at fully converged stable minima and included a series of small steps along the reaction coordinate, with all other degrees of freedom fully optimized. The stationary points have been optimized and verified to have zero negative frequency. The TS structures were obtained from the LT calculations refined with a standard TS search and verified to have exactly one imaginary frequency for a vibrational mode aligned with the reaction coordinate. All intermediates and transition states (TSs) have been calculated using the Gaussian 16 package.[46] The calculations were carried out with the B3LYP exchange−correlation functional plus D3BJ dispersion correction[47,48] and the triple-zeta plus additional polarization function basis set, 6-311G**. The Gibbs free-energy profiles were calculated at 298 K and 1 atm in the solution phase, using the self-consistent continuum approximation (with the default PCM parameterization) of a range of solvents, including dioxane, tetrahydrofuran (THF), Et_2O and Ph_2O for the corresponding ethereal LBs, and toluene for tBu$_3$P and Me$_3$P. All relative energies, including free and potential energies, have been calculated with respect to free LA, LB, and H_2 molecules.

3. COMPOUNDS

3.1. Boron-Based Lewis Acids. Figure 1 shows the 12 LAs considered here, divided into three different categories. In Figure 1A, BCF (**1**) is the most commonly used LA in FLP chemistry, and structures **2**−**6** are derived from BCF by replacing the F atoms with CF_3 groups in the meta and para positions (**2** and **3**) and with H and Cl atoms of entire rings (**3**, **4**, **5**, **6**). In structures **7**−**10**, the effect of front- and back-strain is altered by the addition of the bulkier Cl atom in 2, 3, and 6 positions of one aryl ring while decreasing the number of F atoms. Here, front-strain refers to the shielding of the boron atom by bulky groups that prohibit the interaction of B with the LB, whereas back-strain means prevention of pyramidalization of the BCF-derivative structure, i.e., increase of the deformation energy of the LA structure. Structure **11** has the bulkiest LA-containing C−H groups around B, and structure **12** is included because it forms the classic LA−LB dative bonds with all LBs, so that the strength of the dative bond can be used as a measure of Lewis basicity for the various LBs.

Using this series of LAs, we can analyze the electronic and structural effects on the LA−LB complexation by systematically reducing the number of electronegative F atoms on the rings and by adding bulky groups that increase the pyramidalization strain of the flat BCF. We will thus investigate the LA−LB binding/complexation energy in the initial molecular complex (adduct), the change in Lewis acidity, the hydride affinity and electrophilicity, the role of the deformation (strain) in the structure of the LAs and LBs, and the electronic repulsion between the LA and LB during complexation. Next, we compute these properties during the activation of H_2 and the formation of the transition state (TS) and examine their influence on the $\Delta G^{\ddagger}$ of the H_2 activation (i.e., on the reaction kinetics) and on the overall ΔG (i.e., the thermodynamics of the reaction).

Recent experiments have shown that boron LAs are also able to activate H_2 in combination with ethereal solvents and catalyze hydrogenation reactions.[7−9,36] The produced protons transfer to carbonyl oxygens to form alcohols. This reaction may take place through various mechanisms.[49] Instead, when the Lewis base is P-bearing, the reactivity is much less because the P−H bond is too strong in the precursor of the LA−$H^{(-)}\ldots{}^{(+)}$H−LB ion pair. Finally, the smallest LA and LB in the series, B$(CF_3)_3$ and Me$_3$P, respectively, lead to understanding the extent of Lewis basicity and acidity of the pairs because they form a classical dative LA−LB bond with the other partners in the series.

3.2. Tris(perfluorotolyl)borane, B(p-$C_6F_4CF_3)_3$: A Boron Lewis Superacid. According to recent experimental reports, the tris-(perfluorotolyl)borane, **2**, is a super Lewis acid. It has more acidic character than BCF, and it is the most Lewis acidic single-site triorganoborane.[43] The strong electron withdrawal of the p-$C_6F_4CF_3$ groups, due to the presence of the CF_3 groups at the para positions, strongly affects the H^- affinity. In addition, the para positions of the CF_3 groups do not induce significant deformation strain in the structure of the LA, and this makes it a very strong LA (see also Table 1). In agreement with the experiment, we find that this new highly electrophilic boron-based Lewis acid is an interesting component to access novel reactivity in FLP chemistry.[43] However, due to the strong H^- affinity of this super Lewis acid, it may serve as a poor H^- donor in hydrogenation reactions.

3.3. Influence of the Structural and Electronic Characteristics of Lewis Acids on Complexation to Lewis Bases. We focus our attention on the following ethereal O-based LBs: 1,4-dioxane (dioxane hereafter), tetrahydrofuran (THF), diethyl ether (Et_2O), and diphenyl ether (Ph_2O), all of which have been used experimentally for hydrogenation of C═O bonds.[7−9,36] For comparison, we include two prototypical P-bearing LBs: tBu$_3$P and Me$_3$P. Me$_3$P is a rather small molecule in comparison with tBu$_3$P and forms a strong classical LA−LB dative bond with all LAs, except the bulkiest one (compound **11**), and therefore provides a measure to

https://dx.doi.org/10.1021/acs.jpca.0c03108
J. Phys. Chem. A 2020, 124, 6399−6410

Table 1. H^- Affinity of the LAs in Class A (See Figure 1) and Their Complexation Energies with tBu_3P, Me_3P, THF, and Ph_2O[a]

		($\Delta E_{strain-LA}$)			
LA	H^- affinity	tBu_3P	Me_3P	THF	Ph_2O
1	0.0	−19.9	−31.7 (24.5)	−20.0	−17.9
2	−12.6	−20.8	−36.9 (24.6)	−26.7	−17.0
3	0.5	−19.7	−28.3 (31.7)	−21.8	−19.0
4	1.2	−15.9	−21.7 (31.5)	−14.1	−16.2
5	−0.4	−12.5	−16.0 (34.4)	−10.4	−16.0
6	−1.1	−13.3	−7.5 (40.6)	−8.9	−16.8

[a]All values are in kcal/mol. The hydride affinity is defined relative to that of BCF (see the text). We quantify the Lewis acidity here as the complexation energy of the LA with Me_3P (column four). The numbers in parentheses show the deformation energy in the LA structure due to complexation.

evaluate the strength of the various dative adducts and of the Lewis acidity of the series of LAs. On the other hand, $B(CF_3)_3$ is a small LA that forms a dative bond even with the bulkiest LB and can therefore serve to quantify the Lewis basicity of LBs.

4. RESULTS AND DISCUSSION

4.1. LA−LB Complexation. Tables 1−3 show the complexation energies, $\Delta E^{complex}$ (in kcal/mol), of the initial molecular complexes formed between each LA and four of the six LBs (results for the other two LBs, dioxane and Et_2O, are reported in Table S1 in the Supporting Information (SI)). In addition, the second column shows the hydride affinity of each LA relative to that of BCF, which is calculated as the reaction energy of the reaction: BCF−H^- + LA → BCF + LA−H^-. These H^- affinities may be compared to experimentally determined LA electrophilicities.[23]

Table 2. H^- Affinity of the LAs in Class B (See Figure 1) and Their Complexation Energies with tBu_3P, Me_3P, THF, and Ph_2O[a]

		($\Delta E_{strain-LA}$)			
LA	H^- affinity	tBu_3P	Me_3P	THF	Ph_2O
7	10.8	−12.1	−22.8 (28.8)	−13.2	−12.8
8	8.3	−12.3	−22.8 (29.9)	−12.8	−12.9
9	17.4	−12.3	−20.9 (28.6)	−12.7	−14.2
10	14.5	−14.8	−20.9 (29.7)	−10.6	−11.9

[a]All values are in kcal/mol. The hydride affinity is defined relative to that of BCF (see the text). We quantify the Lewis acidity here as the complexation energy of the LA with Me_3P (column four). The numbers in parentheses show the deformation energy in the LA structure due to complexation.

Table 3. H^- Affinity of the LAs in Class C (See Figure 1) and Their Complexation Energies with tBu_3P, Me_3P, THF, and Ph_2O[a]

		($\Delta E_{strain-LA}$)			
LA	H^- affinity	tBu_3P	Me_3P	THF	Ph_2O
11	4.9	−12.5	−7.65 (5.5)	−9.23	−15.77
12	−26.9	−53.2	−66.13 (23.0)	−52.43	−36.53

[a]All values are in kcal/mol. The hydride affinity is defined relative to that of BCF (see the text). We quantify the Lewis acidity here as the complexation energy of the LA with Me_3P (column four). The numbers in parentheses show the deformation energy in the LA structure due to complexation.

Complexation of an LA and an LB can either lead to dative bond formation between the donor and acceptor centers or, if steric hindrance of the ligands prohibits the LA and LB centers to come close enough, to the formation of a van der Waals complex, i.e., a frustrated Lewis pair (FLP). The interaction energies for these two kinds of complexes are typically in the same range, but the distance between the LA/LB centers is very different, either equal to a covalent bond length or longer than ca. 3.8 Å. See Figure 2 (top panel) for the illustrations of both types of structures. Van der Waals adducts of bulky LBs and LAs with long, 3.8−6.0 Å, donor−acceptor distances require strong dispersion interactions to stay together. Instead, small dative bond-forming pairs interact mainly through electrostatic and orbital interactions and with stronger repulsive interactions between the occupied orbitals of the LA and LB fragments, inducing larger deformation of the LA and LB structures. Me_3P and THF form dative adducts with all LAs, except **11**, whereas tBu_3P and Ph_2O form a dative adduct with none of the LAs.

Taking the prototypical BCF structure (**1**) as our reference, replacement of the F atoms in the para position with CF_3 groups (**2**) has a significant effect on the H^- affinity (note that a negative number means a stronger affinity than that of BCF). Since the deformation in the LAs **1** and **2** is similar, the stronger complexation energy between **2** and Me_3P or THF is due to electronic effects. On the other hand, removing the F atoms from one ring and adding two CF_3 groups on the meta positions (**3**) weakens the H^- affinity somewhat and, due to the increased LA structure deformation in complex formation, it is less Lewis acidic than **1**.

Replacing the F atoms by Cl atoms on one ring (**4**), two rings (**5**), and three rings (**6**) decreases the strength of the dative adduct with Me_3P with each additional ring due to the increasing deformation energy. The opposite trend is seen for the H^- affinity, although the affinity first decreases with structure **4**. By varying the amount and type of substitution, it is possible to tune the strength of the dative adduct from −36.9 to −7.5 kcal/mol. Instead, in the case of the van der Waals complexes, the differences in complexation energy are not so large. In the van der Waals complexes with tBu_3P and Ph_2O, the stabilization is largely due to dispersion interaction, while deformation and repulsion are less important because of the larger distance between the LA and LB centers compared to those with Me_3P and THF.

These dominant attractive dispersion interactions are similar for tBu_3P and Ph_2O regardless of the fact that one is a P-bearing LB and the other is an O-bearing LB. The interaction between a solvent (ethereal) LB and an LA is seen to be rather strong. Hence, the preparation (reorganization) energy of the LA and LB pairs for the H_2 activation in the van der Waals adducts of tBu_3P and Ph_2O is similar.

Table 2 shows the results for the LA structures in class B (see Figure 1B) that were derived from BCF by replacing the F atoms with H and Cl atoms to measure the effect of front-strain (positions 2 and 6 in the aryl rings) and back-strain (position 5). The H^- affinity of all four LAs is much decreased compared to that of the original BCF structure, and the Lewis acidity to form a dative bond with Me_3P is decreased by up to ca. 35% (also, with THF a dative bond is formed). The complexation energy with tBu_3P and Ph_2O, with which the LAs

https://dx.doi.org/10.1021/acs.jpca.0c03108
J. Phys. Chem. A 2020, 124, 6399−6410

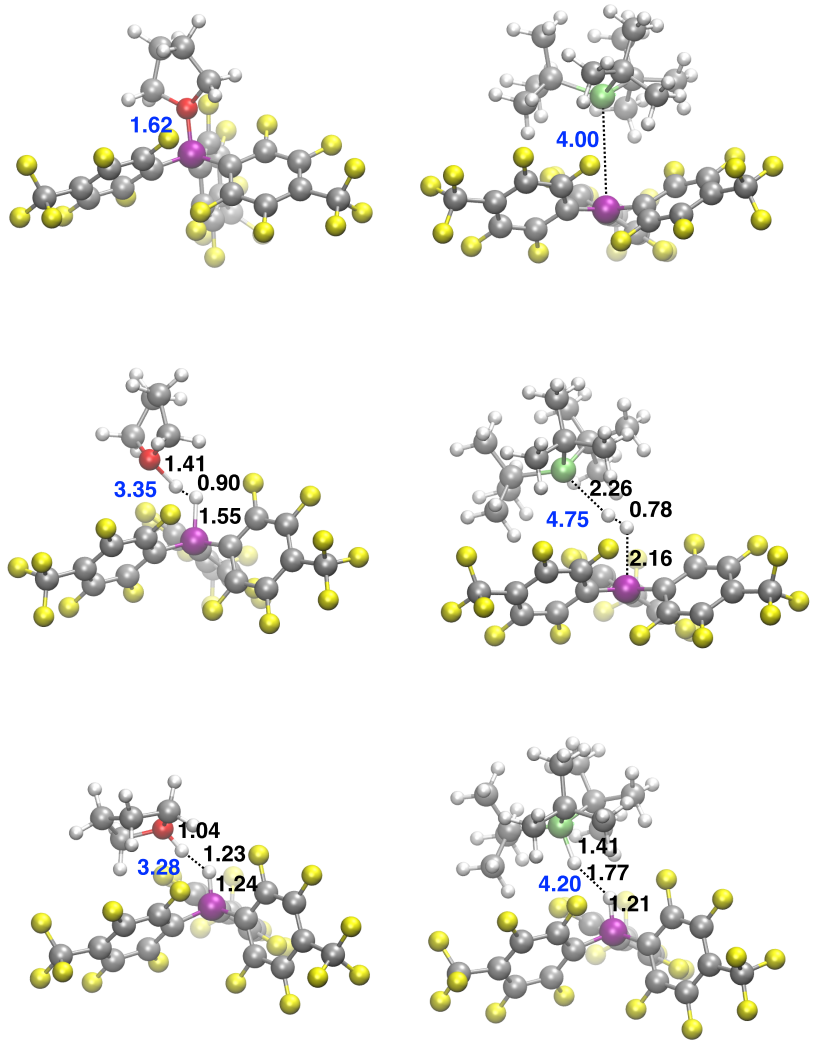

Figure 2. Optimized structures of two representative frustrated Lewis pairs at key stages during the H_2 activation: the dative bond forming the tris(perfluorotolyl)borane/THF pair (left) and the van der Waals complex forming the tris(perfluorotolyl)borane/tBu$_3$P pair (right). Top: empty initial complexes; middle: transition states; and bottom: product states. Distances (in Å) for O−H or P−H, H−H, and H−B are shown in black font; O−B or P−B distances are shown in blue.

form a van der Waals complex, is similar to that of THF. Addition of one Cl atom at position 5 (see structures **8** and **10** versus **7** and **9**) results in a stronger H^- affinity by 2.5−3 kcal/mol. LAs **9** and **10** are weak H^- acceptors, and their corresponding LA−$H^{(-)}$...$^{(+)}$H−LB ion pairs are known to release H_2. The back-strain results in a larger deformation in the LA structure; its effect on decreasing the complexation energy is more visible with less donating LBs such as THF.

Table 3 presents the data of the bulkiest and the strongest alkylated LAs, **11** and **12**, respectively. In **11**, the congestion around the boron atom is large. The C−H bonds are almost perpendicular to the BCCC plane so that the hydrogens shield the boron. According to previous experimental investigations, considerable steric shielding of the boron center imparted by the large $CH(C_6F_5)_2$ ligands hinders access to the Lewis base and results in a weak borane LA.[41] The H^- affinity of **11** is nevertheless stronger than that of the LAs of class B. This means that the C_6F_5 rings can induce their electronegativity to the B atom despite the extra C−H groups and make it more electrophilic than the class B LAs. None of the LBs form a dative bond with **11**. The complexation energy of **11** with tBu$_3$P is similar to that of the class B LAs. Instead, **12** forms a dative bond with all LBs, showing the strongest interaction with Me_3P.

The Lewis basicity of the LBs can be estimated from the strength of the dative bond to **12**.

In Figure 3, we plot the calculated LA−LB complexation energies, $\Delta E^{complex}$, versus the LA−LB distances. Two categories of complexes can be distinguished based on the LA−LB distances: the ones with a dative LA−LB bond, grouped on the left in the plot with distances between 1.6 and 2.3 Å, and the ones forming the van der Waals complexes, seen on the right with distances from 3.8 to 6.0 Å. For the first group, the dative bond distance is ca. 1.7 Å along the whole group of O-bearing LAs and ca. 2.2 Å for the P-bearing LAs. The substantial variation in $\Delta E^{complex}$ in this group is due to the large differences in structure deformation needed to form the compact molecular complexes, resulting in a steep, near-linear, correlation between the LA−LB distance and the complexation energy.

Instead, the second group, mainly FLP complexes containing tBu$_3$P and Ph_2O, is distributed horizontally, i.e., their complexation energy is near the average of 14 kcal/mol, but the LA−LB distances show large variations, illustrating the

https://dx.doi.org/10.1021/acs.jpca.0c03108
J. Phys. Chem. A 2020, 124, 6399−6410

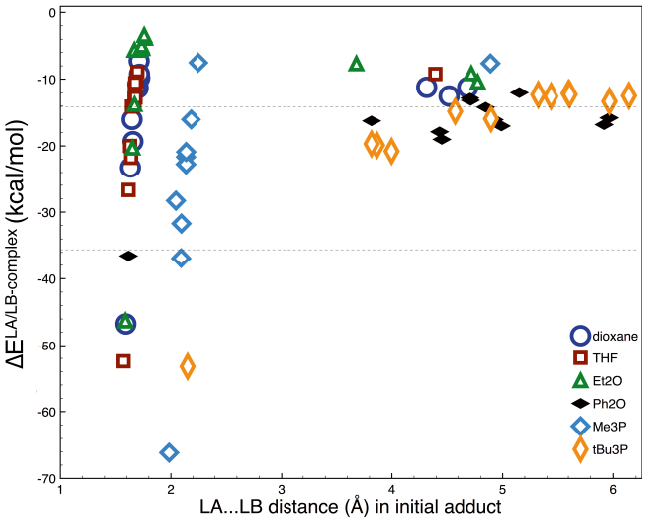

Figure 3. Complexation energies (in kcal/mol) of the initial molecular complexes formed between LA and LB versus the LA···LB distances (in Å). Two groups can be distinguished: dative LA−LB bond formers (left) and VdW complex formers (right).

flexibility of these molecular complexes, while the van der Waals interaction energy shows remarkably little variation. The relative values of complexation free energies of the initial complexes are reported in Table S2 in the SI. Addition of diffuse functions to the basis set (e.g., 6-311++G**) results in slightly endergonic complexation free energies for the initial LA···LB VdW complexes, including tBu$_3$P (the values are reported in Table S2 in the SI).

The conformational complexity of the initial VdW complexes has been the subject of molecular dynamics investigations, which illustrate the feasibility of several energetically low-lying structures.[50,51] Using the conformer rotamer ensemble sampling tool (CREST) code,[52,53] conformers of the initial VdW complexes of tBu$_3$P···LA 2 (strong LA) and tBu$_3$P···LA 8 (weak LA) have been generated within 2 kcal/mol. The total number of conformers are 34 and 44 for LA **2** and LA **8**, respectively, which indicates the flexibility of these VdW complexes. The variation of the relative energy versus the B···P distance (Å) is presented in Figure 4. The VdW complexation between tBu$_3$P and LA **8** generates more number of conformers than the VdW complexation between tBu$_3$P and LA **2**, which indicates the effect of weaker interaction in the former case.

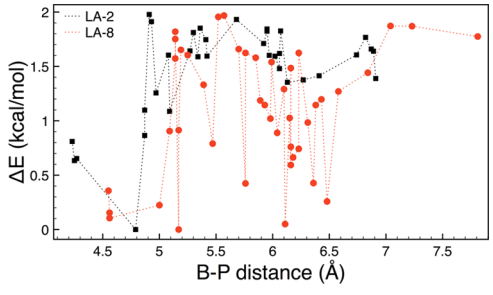

Figure 4. Variation of the relative energies (kcal/mol) versus the B···P distance (Å) for the generated VdW complexes (within 2 kcal/mol) of tBu$_3$P···LA 2 (black) and tBu$_3$P···LA 8 (red). For generation of conformers, the CREST method, which is a metadynamics-based conformer generation tool, has been used.

In this study, the focus is on the relative trends within various LA/LB categories, and free energies of the transition states and reactions are calculated versus the free molecules. Hence, the final results are not influenced by the slight variation in complexation free energies of the initial molecular complexes due to the basis set or conformational flexibility.

4.2. Transition-State Barriers of H_2 Activation. We proceed our study with the H_2 activation reaction catalyzed by each of the LA−LB complexes discussed in the previous section. First, we examine the free-energy barrier, $\Delta G^{\ddagger}$, of the heterolytic H_2 dissociation and binding to the Lewis pair (see reaction 1), and in the section hereafter, we discuss the overall reaction free energy, ΔG. All free energies are relative to the sum of the free energies of the isolated LA, LB, and H_2 fragments. See Figure 2 (middle panel) for representative illustrations of two optimized transition-state structures associated with the computed free-energy barriers. The main focus in this section is on highlighting the individual roles of the LA and LB in the reaction kinetics.

Figure 5 shows the $\Delta G^{\ddagger}$ for all LA/LB complexes, arranged by the LA structure index (see Figure 1) on the x-axis.

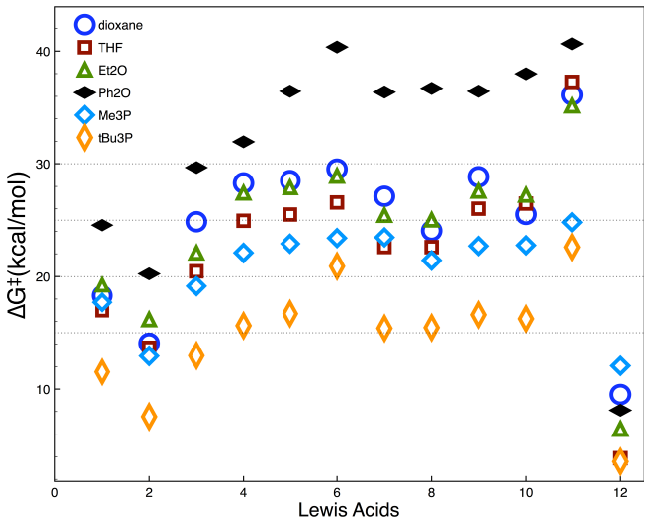

Figure 5. H_2 activation free-energy barrier, $\Delta G^{\ddagger}$, for all FLP complexes ordered by Lewis acid (see Figure 1 for LA numbering).

Comparison of LA structures **1**, **2**, and **3** shows an electronic effect on $\Delta G^{\ddagger}$: F/CF$_3$ substitution at the para positions (**2**) lowers the barrier by 4.5 kcal/mol, and a partial F/H and F/CF$_3$ substitution (**3**) leads to an increase of $\Delta G^{\ddagger}$ by ca. 6 kcal/mol.

Replacing F atoms with Cl atoms (**4**−**6**) increases $\Delta G^{\ddagger}$; e.g., with THF as the LB, the barrier increases from 20.5 to 26.6 kcal/mol. Thus, replacing all three C$_6$F$_5$ rings by C$_6$Cl$_5$ rings makes the borane Lewis acid kinetically less potent of splitting the H_2 molecule, although the H$^-$ affinity of **6** is stronger than that of BCF (see Table 2). Another structural effect is seen from **6** to the group of **7**−**10**: the $\Delta G^{\ddagger}$ decreases ca. 5.0 kcal/mol, e.g., with tBu$_3$P. The LAs **6** and **11** have the highest steric hindrance around the boron center in the LA series, and the highest $\Delta G^{\ddagger}$ corresponds to these LAs. This effect has been observed experimentally with the elevated temperature required for the H_2 activation with LAs **6** and **11**.[36,41] Hence, we see that the bulkiness and structural congestion around the boron center increase the barrier height. Note that the opposite effect is seen for the LBs; e.g., the bulky tBu$_3$P

https://dx.doi.org/10.1021/acs.jpca.0c03108
J. Phys. Chem. A 2020, 124, 6399−6410

shows with all LA partners a lower barrier for H_2 splitting than Me_3P.

We note that, although highly Lewis acidic boranes with strong H^- affinity provide facile H_2 activation, e.g., **1** and **2**, the resultant B−H bonds (borohydride anions) are consequently poor hydride donors that can limit the scope of substrates to be reduced in the hydride transfer step. A major factor in determining the kinetic ability of FLPs to cleave H_2 is the combined Lewis acidity and basicity of the system: when both are strong as in the case of tBu$_3$P and LAs **1** and **2**, the activation barrier is minimal. Since the Bronsted basicity of the ethereal solvents is substantially lower relative to the typical amine or phosphine bases commonly utilized in FLP chemistry, our results indicate that, in order for the system to activate H_2 with a moderate activation barrier, the hydride affinity of the LA must be strong, as seen from LAs **1** and **2**, which have the lowest barrier with ethereal solvents. This is in agreement with the experimental observation that borane LAs with fewer F atoms are less reactive toward H_2 activation.[38,41] One can conclude that structures **7** and **8** in group B are the most efficient LAs in combination with ethereal solvent molecules since they have a moderate barrier of H_2 activation (not too high) and the H^- affinity is also not too strong to prohibit further hydride donation for the subsequent C═O hydrogenation. This is in line with the experimental observation that only **7** and **8** in group B can produce alcohol from an olefinic ketone.[38]

Concerning the individual role of the LB, a comparison of the barriers of Me_3P and tBu$_3$P shows that FLPs containing tBu$_3$P have on average a 5 kcal/mol lower barrier. This illustrates the impact of the LB bulkiness on the barrier of H_2 activation. According to a previous study,[54] the attractive interactions increase at the TS due to the closer distance between the LA···LB pocket and H···H fragment. However, the repulsive interactions and the deformation in the structures of the FLP fragments also increase. The smaller LBs need to be closer to H···H to polarize H_2 and reach the balance between attractive and repulsive interactions, and this by itself means a later TS along the reaction path and a higher barrier. In the case of a strong and bulky LB, like tBu$_3$P, the activation of H_2 takes place in an earlier position along the reaction coordinate, i.e., a larger LA···LB pocket and a longer distance between the LA/LB centers and the H···H fragment. Hence, for smaller LBs, the barrier height is controlled by electronic effects (frontier molecular orbitals), and for bulky LBs, the barrier height is under the control of steric effects. In FLPs with the bulky tBu$_3$P, the distance between the LA···LB centers in the TS structure is 4.3−5.3 Å and with Me_3P 4.0−4.3 Å. THF and Et_2O have distances within 3.2−4.0 Å, and TSs with dioxane have the shortest LA···LB distances, of 3.0−3.2 Å. We note that a larger size of the LA···LB pocket is connected to a shorter H···H distance and an earlier transition state. The complete geometrical parameters of the TS structures, including LA···H, H···H, and H···LB, are reported in the SI, Table S9. Figure S10 in the SI shows the correlation between $\Delta G^{\ddagger}$ and LA···LB distances in the TS structures.

From the O-bearing LBs, THF is the strongest (the most nucleophilic) one; i.e., THF has the lowest barrier of, on average, ca. 22 kcal/mol. Dioxane and Et_2O have similar average barriers of ca. 25 kcal/mol. Ph_2O is the least nucleophilic ethereal LB, with a 0.5 eV lower highest occupied molecular orbital (HOMO) than the other ethers, and has the highest average $\Delta G^{\ddagger}$ of ca. 32 kcal/mol. This explains why Ph_2O is not an experimentally efficient ethereal solvent for hydrogenation of C═O compounds. Moreover, Ph_2O is a very weak LB and is known to produce an unstable LA−$H^{(-)}$...$^{(+)}$H−LB ion pair.[7] The order of $\overline{\Delta G^{\ddagger}}$ is thus tBu$_3$P < Me_3P < THF < dioxane ≅ Et_2O < Ph_2O. We note that the values of proton affinities of this series of LBs are 252.2, 233.0, 208.0, 200.8, 202,0, and 197.6 kcal/mol, respectively. Regarding the individual role of the LBs, the bulkiness of the LB (tBu$_3$P versus Me_3P) and nucleophilicity (P−LBs versus O−LBs) affect most strongly the barrier of H_2 activation. Concerning the nucleophilicity, we note that the HOMO level of phosphine LBs is 1.0 eV higher than that of oxygen−LBs.

A comparison between the B···H and H···LB distances in the TS structures shows that the covalent bond formation in P-bearing LBs is earlier for the B···H bond than for the H···P. However, in O-bearing LBs, the H···O bond forms earlier than B···H. For example, in Figure 2, for THF, the B···H and O···H distances at the transition states are 1.55 and 1.41 Å, respectively, and for tBu$_3$P, the B···H and P···H distances are 2.16 and 2.26 Å, respectively. As can be seen in Figure 2, in the case of FLPs with tBu$_3$P, the TS is earlier than with THF; i.e., the H···H distance is 0.78 Å versus 0.90 Å, respectively. The H···H distance in H_2 is 0.75 Å.

4.3. Interactions between H_2 and FLPs. To analyze the interactions between H_2 and FLPs, four representative categories out of 75 FLPs have been selected, including strong LB−strong LA, strong LB−weak LA, weak LB−strong LA, and weak LB−weak LA. Figure 6 shows the transition-state

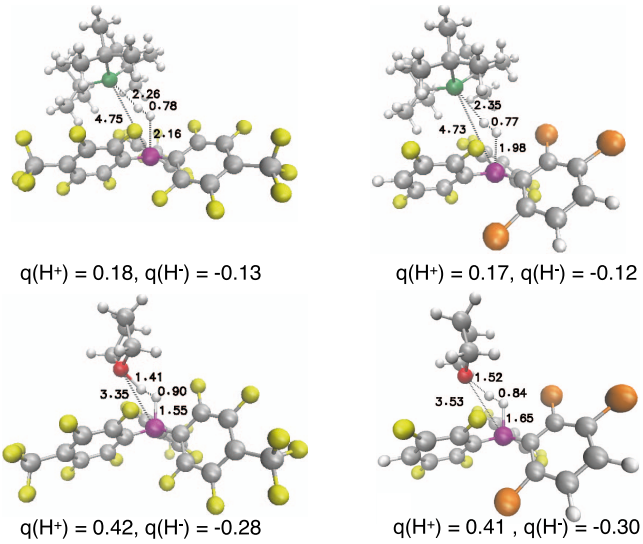

Figure 6. Transition-state structures of the four selected models of FLPs, including tBu$_3$P−LA **2**, tBu$_3$P−LA **8**, THF−LA **2**, and THF−LA **8**. The important distances are depicted in Å. Mulliken atomic charges of H^+ and H^- are shown in brackets.

structures of these models, including tBu$_3$P−LA **2**, tBu$_3$P−LA **8**, THF−LA **2**, and THF−LA **8**. The important distances are depicted in Figure 6. We note that Bu$_3$P is a strong LB and LA **2** is a strong LA. On the other hand, THF and LA **8** are weak LB and LA, respectively. The Mulliken atomic charges of H^+ and H^- have been presented to illustrate the electronic charge localization on H^+···$^-$H at the transition state. Larger positive/negative atomic charges on the H^+···$^-$H mean more separation of H^+···$^-$H or later transition-state character. Figure 6 indicates that for a strong LB (tBu$_3$P), stronger LA **2**

https://dx.doi.org/10.1021/acs.jpca.0c03108
J. Phys. Chem. A 2020, 124, 6399−6410

produces a transition state with a longer B···H distance of 2.16 Å and a weaker LA **8** shorter B···H distance of 1.98 Å. On the other hand, for a weak LB (THF), the situation is opposite and the stronger LA **2** produces a shorter B···H distance, which indicates stronger interaction between B and H atoms.

More details of the impact of the electronic and structural properties of the LAs on the frontier molecular orbital (FMO) interactions between FLPs and H_2 have been analyzed using HOMO−lowest unoccupied molecular orbital (LUMO) gaps at the transition-state structures of the four models of FLPs. As shown in ref 48, the frontier molecular orbitals (FMOs) of the transition-state structures of FLPs can arise not only from the "push−pull" molecular orbital scheme (case 1 in Figure 7) but

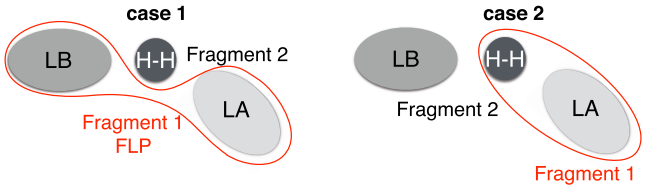

Figure 7. $[LB\cdots H\cdots H\cdots LA]^{TS}$ transition state from the viewpoint of the EDA method; considered fragmentation schemes for Table 4 (case 1) and Figure 8 (case 2).

also from the more intricate but energetically more fitting orbital interactions. The reported results in ref 48 indicate that a combination of HOMO[LB + H_2] interacting with LUMO[LA] and LUMO[LA + H_2] interacting with HOMO-[LB] is viable. In the push−pull molecular scheme, pure occupied σ and empty σ*MOs of H_2 are involved. Since in the present work the focus is on the properties of the LAs, we have selected LUMO[LA + H_2] interacting with HOMO[LB] (case 2 in Figure 7) to analyze the HOMO−LUMO gaps. Hence, the LA + H_2 is considered as a single fragment. Figure 8 shows the HOMO−LUMO gap for the four selected categories of FLPs. Figure 8 indicates that the stronger LB (tBu$_3$P) has a lower HOMO[LB]−LUMO[LA + H_2] gap than the weaker LB (THF). Furthermore, in the case of strong LB and strong LA, the HOMO[LB]−LUMO[LA + H_2] gap is the lowest. In the case of weak LB (THF), the HOMO[LB]−LUMO[LA + H_2] gap is ca. 1 eV larger than the corresponding cases of strong LB.

Interactions between H_2 and FLPs at the transition state have been analyzed using the EDA method; the details are explained in the SI.[55,56] EDA results (at the B3LYP-D3/TZP level of theory) for case 1 in Figure 7 are reported in Table 4. In Table 4, $\Delta E_{Pauli}^{\ddagger}$ is the interaction between the occupied molecular orbitals and is responsible for the steric repulsion, $\Delta E_{elstat}^{\ddagger}$ is the classical electrostatic interaction, and $\Delta E_{steric}^{\ddagger}$ is the sum of $\Delta E_{Pauli}^{\ddagger}$ and $\Delta E_{elstat}^{\ddagger}$. $\Delta E_{oi}^{\ddagger}$ is the orbital interaction that accounts for the charge transfer between the HOMO and LUMO of two fragments; finally, $\Delta E_{disp}^{\ddagger}$ is the dispersion energy due to the van der Waals attractions. $\Delta E_{int}^{\ddagger}$ is the sum of the electrostatic, Pauli, and orbital interactions plus dispersion contribution.

As reported in Table 4, lower steric repulsion in [tBu$_3$P + LA 2]···H_2 and [tBu$_3$P + LA 8]···H_2 accounts for a lower barrier than their counterparts with THF, i.e., 7.5 and 15.4 kcal/mol versus 13.6 and 22.6 kcal/mol, respectively. In the case of [tBu$_3$P + LA 2]···H_2 and [tBu$_3$P + LA 8]···H_2, orbital interactions in combination with dispersion attractions overcome the positive steric repulsion and result in an attractive

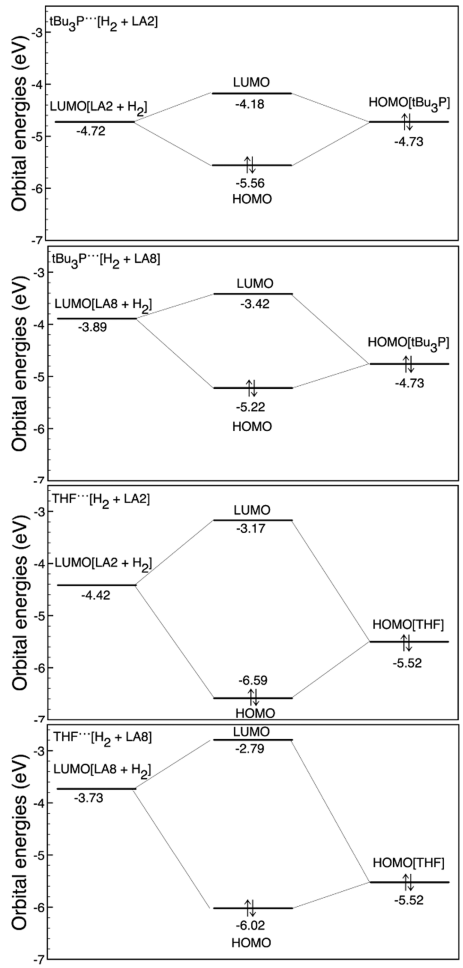

Figure 8. HOMO[LB]−LUMO[LA + H_2] gap for the four selected categories of FLPs in Figure 6 at the transition states. As the LUMO, we have shown the combined LUMO[LA + H_2], where the LA + H_2 is considered as a single fragment.

interaction between H_2 and FLP. In the case of [THF + LA 2]···H_2 and [THF + LA 8]···H_2, although the rather large steric repulsions are canceled by the strong orbital interactions, the barrier is larger than that of FLPs with tBu$_3$P due to the late transition-state character (closer to the product structures). The strongest interaction that can be observed in the FLP consists of THF and LA **2** (−17.72 kcal/mol), which has the shortest B···H distance at the transition-state structure (Figure 6), and the dispersion interactions have only a minor effect versus orbital interactions. Hence, the driving force for H_2 splitting, that is, the interactions between H_2 and LA and LB, depends on the electronic properties of the FLPs.

4.4. Roles of the Lewis Acid and Base in the Thermodynamics of H_2 Activation. In this section, we discuss the electronic and structural effects of the Lewis pairs on the reaction free energy, ΔG, of the H_2 activation leading to the formation of the LA−$H^{(-)}\cdots^{(+)}$H−LB product ion pairs (see reaction 1). The upper panel in Figure 9 shows ΔG versus the $H^{(-)}\cdots^{(+)}$H distance in the product complex. For the sake of brevity, we only show the results for the FLPs formed from the LBs tBu$_3$P, Me$_3$P, and THF paired with each of the LAs shown in Figure 1. The longest $H^{(-)}\cdots^{(+)}$H distances are related to the bulkiest LB, tBu$_3$P, which is seen to form on average the most stable product ion pairs. Thus, the stability of the ion pair is largely controlled by the LB. The order of the

https://dx.doi.org/10.1021/acs.jpca.0c03108
J. Phys. Chem. A 2020, 124, 6399−6410

Table 4. EDA Results (kcal/mol) for the FLP Fragment [LA + LB] Interacting with H_2 for the Transition-State Structures Shown in Figure 6

[LA + LB]···H_2	$\Delta E_{int}^{\ddagger}$	$\Delta E_{Pauli}^{\ddagger}$	$\Delta E_{elstat}^{\ddagger}$	$\Delta E_{oi}^{\ddagger}$	$\Delta E_{steric}^{\ddagger}$	$\Delta E_{disp}^{\ddagger}$
[tBu_3P + LA 2]···H_2	−3.92	41.88	−14.17	−26.29	27.71	−5.35
[tBu_3P + LA 8]···H_2	−2.17	44.50	−15.07	−25.84	29.43	−5.77
[THF + LA 2]···H_2	−17.72	133.01	−48.93	−96.34	84.08	−5.46
[THF + LA 8]···H_2	−5.51	99.82	−36.92	−63.03	62.90	−5.38

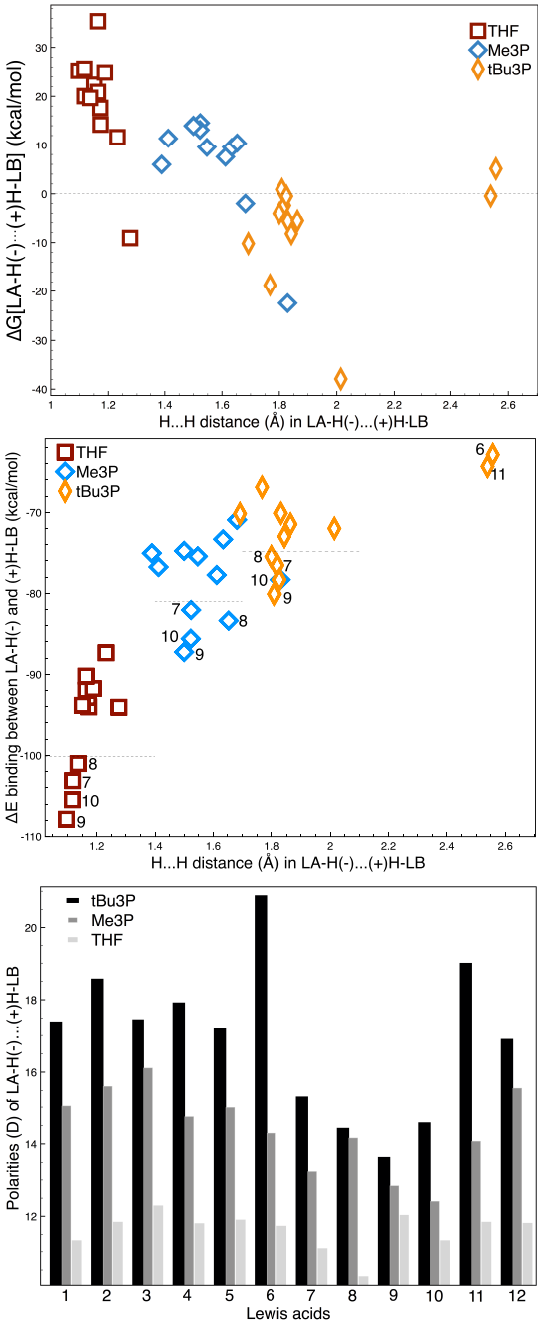

Figure 9. ΔG (top panel) and the $\Delta E^{binding}$ (middle panel) of the product ion pair versus the H···H distance. Bottom: the polarity (in Debye) of the ion pairs of THF, Me_3P, and Bu_3P with each of the LAs.

product ion pair stability is tBu_3P > Me_3P > THF. For ion pairs with tBu_3P, the ΔG is negative in most of the LPs. Instead, for Me_3P and THF, the ΔG is always positive (except with LA **12** and LA **2** for Me_3P) and larger for THF LPs. The shorter $H^{(-)}...^{(+)}H$ distance corresponds to a higher ΔG and a less stable ion pair (i.e., a more reactive species for the subsequent hydrogenation).

There is a correlation between the binding energy between the cationic and anionic fragments in the product complex and the $H^{(-)}...^{(+)}H$ distance, which is shown in the middle panel of Figure 9. Here, the binding energy is computed as the energy difference between that of the product complex and of the separated (i.e., isolated) LA−$H^{(-)}$ and $^{(+)}$H−LB fragments. The bulkier and stronger LB, tBu_3P, shows after protonation the weakest binding interaction with the LA−$H^{(-)}$ fragments compared to the Me_3P and THF LBs. The larger the charge separation, the less negative is the binding energy. THF, which is the weakest base of the three, shows the strongest binding interaction and the shortest charge separation. The binding energy is mainly composed of the very negative electrostatic interaction energy, which scales as the Coulomb law with the reciprocal distance, and the positive steric repulsion that has, in first approximation, a faster decaying exponential scaling with the distance. Bulkier fragments have a larger cavity and allow for a larger $H^{(-)}...^{(+)}H$ charge separation.

Also, the hydride affinity of the LA plays a role in this correlation, which is illustrated by the labeled group of Lewis acids **7**−**10** in the middle panel. These LAs have the most negative binding energy with each of the three Lewis bases, which correlates with the weakest H^- affinity, in the order of **9**, **10**, **7**, and **8**, as listed in Table 2.

The weaker H^- affinity allows for a somewhat shorter $H^{(-)}...^{(+)}H$ distance and thus a more attractive electrostatic interaction between the cationic and anionic fragments in the ion pair.

In the lower panel of Figure 9, we show the polarities of the ion pairs. From THF to tBu_3P, the polarity of the ion pairs increases, which correlates with the larger charge separation inside the ion pair. Thus, the polarity correlates to the proton−hydride distance, which is controlled by the bulkiness of the LB. A highly polar product ion pair can be further stabilized by solvation effects in a polar solvent.[57] However, the O-bearing LBs, such as THF, do not form very polar product ion pairs, so that solvation stabilizes the ion pair molecule only by a few kcal/mol, which is not enough to change the sign of the ΔG of the reaction.

In sum, the thermodynamic picture of the H_2 activation as drawn by Figure 9 shows that the most stable product ion pair with respect to the LA, LB, and H_2 reactants is formed by the bulky and strong LB fragment, which leads to a negative or moderately positive reaction free energy. Bulkier fragments form complexes with larger cavities, which allow for a larger charge separation and thus an easier-to-separate product complex. However, a too strong LB will form a weak proton donor for the hydrogenation. The Lewis base takes a more pronounced role in the thermodynamics of the H_2 activation, polarity, and stability of the product ion pair than the Lewis acid.

https://dx.doi.org/10.1021/acs.jpca.0c03108
J. Phys. Chem. A 2020, 124, 6399−6410

4.5. Optimizing the Energetics of H_2 Activation.

Figure 10 shows the free-energy profiles of the LA/LB

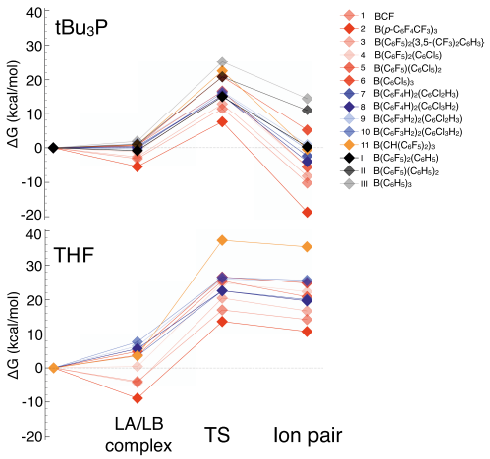

Figure 10. Free-energy profiles of complexation and H_2 activation by FLPs composed of tBu$_3$P (top) or THF (bottom) with LAs **1**−**11**. For tBu$_3$P, three extra LAs, $B(C_6F_5)_2C_6H_5$, $B(C_6F_5)(C_6H_5)_2$, and $B(C_6H_5)_3$, are included with labels I−III. The color saturation correlates with the H^- affinity in each category of LAs.

complexation and the formation of the H_2 activation transition state and ion pair product, with respect to the separated reactants, for tBu$_3$P (top panel) and THF (bottom panel) in combination with the LAs **1**−**11**. For tBu$_3$P, three extra LAs are added by replacing the C_6F_5 rings with C_6H_5 (i.e., $B(C_6F_5)_2C_6H_5$, $B(C_6F_5)(C_6H_5)_2$ and $B(C_6H_5)_3$) to have an extended data set that better illustrates the sign change of the ΔG. For strong LAs, the free-energy profile is exergonic, e.g., for BCF, the ΔG is −10.19 kcal/mol, and for $B(p\text{-}C_6F_4CF_3)_3$, it is −18.60 kcal/mol. The free-energy profile shifts to endergonic for FLPs with weaker LAs; e.g., the ΔG is around 0.30 kcal/mol for $B(C_6F_5)_2(C_6H_5)$ and 14 kcal/mol for $B(C_6H_5)_3$. The $\Delta G^{\ddagger}$ and ΔG show an increasing trend with the decreasing electrophilicity of the LA. The weakest LAs combined with tBu$_3$P show free-energy profiles that resemble those of O-bearing LBs, with barriers around 25 kcal/mol and a ΔG of around 15 kcal/mol.

Table 5 compiles the H···H distance, $\Delta E_{binding}$, ΔG, and $\Delta G^{\ddagger}$ for the FLPs of tBu$_3$P with the three extra LAs and BCF for

Table 5. Values of H···H (Å), $\Delta E_{binding}$, ΔG of the Ion Pair, and $\Delta G^{\ddagger}$ in kcal/mol for the FLPs with the Three LAs, Obtained by Replacing the C_6F_5 Rings with C_6H_5 in Steps, Paired with tBu$_3$P are Shown in Comparison to That of BCF

LA	$H^{(-)}...^{(+)}H$ (Å)	$\Delta E_{binding}$	ΔG	$\Delta G^{\ddagger}$
$B(C_6F_5)_3$	1.69	−70.17	−10.19	11.53
$B(C_6F_5)_2(C_6H_5)$	1.61	−76.02	0.30	15.12
$B(C_6F_5)(C_6H_5)_2$	1.59	−81.19	11.12	20.87
$B(C_6H_5)_3$	1.51	−86.16	14.53	25.26

comparison. By decreasing the electrophilicity of the borane derivatives by replacing F atoms for H atoms, the H···H distance decreases and the $\Delta E_{binding}$ becomes more negative. In line with the discussion of the hydride affinity in the previous section, the decreasing electrophilicity leads to a stronger interaction between the cationic and anionic fragments and a change of the free-energy profile from exergonic to endergonic.

The lower panel of Figure 10 shows the calculated free-energy profiles for FLPs containing THF. With any of the LAs, the H_2 splitting is seen to be endergonic. In class B, **7** and **8** have a somewhat lower free-energy profile than **9** and **10**, and the free-energy difference between the ion pair and the TS is larger for **7** and **8** (ca. 3 kcal/mol) than for **9** and **10** (ca. 0.9 kcal/mol). The larger difference suppresses facile H_2 recombination and provides a longer lifetime of the ion pair for subsequent hydrogenation in **7** and **8**.

Recently, it was found that the free-energy profile may become exergonic through the formation of a particularly stabile "borohydride/hydronium" ion pair intermediate in the presence of water molecules.[58]

The results shown in Figure 10 are in agreement with the "Hammond's postulate" that the transition-state structure in an exothermic reaction resembles the reactants and in an endothermic reaction seems like the products. Furthermore, the barrier heights correlate very well with the reaction free energies of H_2 splitting, which is in accordance with the "Bell−Evans−Polanyi (BEP) principle". In other words, the more exothermic the reaction is, the lower the activation barrier is or *vice versa*.

5. CONCLUSIONS

We have presented a computational study of the process of hydrogen splitting by frustrated Lewis pairs. We have investigated a large set of 75 Lewis pairs. In particular, we have focused our attention on the influence of the structural and electronic properties of the Lewis acids and bases on the activity toward hydrogen splitting. Moreover, the individual roles of the Lewis acid and base in the H_2 activation kinetics and thermodynamics were assessed by considering two series of Lewis bases, including strong phosphine LBs and mildly basic ethereal solvents.

We found that when the Lewis base is strong, as with tBu$_3$P, varying the electronic character of the Lewis acid can modulate the free-energy profile of H_2 splitting from strongly exergonic to strongly endergonic, as shown in Figure 10. For FLPs with a less exergonic energy profile, the LA−$H^{(-)}...^{(+)}$H−LB product ion pair is not stable so that H_2 release may occur before hydrogenation or other follow-up reactions can take place.

In the case of ethereal solvent molecules (O-based LBs), the product ion pair is weakly polar and the cation/anion fragments interact strongly, which makes separation of the fragments for further reactivity energetically unfavorable. Moreover, due to the modest polarization in the complex, solvation does not significantly enhance the stabilization of the ion pair. The larger $H^{(-)}...^{(+)}H$ distance in P-bearing LBs is a result of bulkiness and nucleophilicity, which leads to a product ion pair that is more stable with respect to the reactants, but is at the same time easier to dissociate into the cationic/anionic fragments for subsequent reactivity.

The kinetics (i.e., the barrier height) of the H_2 splitting depends on (1) the bulkiness of the LB and LA fragments, (2) the nucleophilicity of the LB, and (3) the electrophilicity of the LA. Bulkier LBs form a larger cavity in the FLP complex, which results in an early transition state and a lower barrier. On the other hand, bulkiness and steric congestion of the LA hinder the accessibility of the LA center and increase the barrier height. The results of the present work are in good accordance with Hammond's postulate and the Bell−Evans−Polanyi (BEP) principle.

https://dx.doi.org/10.1021/acs.jpca.0c03108
J. Phys. Chem. A 2020, 124, 6399−6410

■ ASSOCIATED CONTENT

Supporting Information

The Supporting Information is available free of charge at https://pubs.acs.org/doi/10.1021/acs.jpca.0c03108.

> ΔG of the initial LA/LB complexes and details of the EDA method; EDA results for the initial molecular complexes between LA and LB; figures of the free-energy profiles of Me_3P, dioxane, and Et_2O; figures of $\Delta G^{\ddagger}$ versus complexation energies of the initial LA−LB complexes and LA···LB distances; ΔG of the product ion pairs in solution; geometrical parameters of the TSs and products, and tables with calculated absolute energies of all structures and imaginary frequencies of the TSs; and the *xyz* coordinates of all structures (PDF)

■ AUTHOR INFORMATION

Corresponding Author

Mojgan Heshmat − *Van't Hoff Institute for Molecular Sciences, Universiteit van Amsterdam, 1098 XH Amsterdam, The Netherlands;* orcid.org/0000-0003-1028-3035; Email: Mojgan.Heshmat@catalyticcenter.aachen-rwth.de, mht780@gmail.com

Author

Bernd Ensing − *Van't Hoff Institute for Molecular Sciences, Universiteit van Amsterdam, 1098 XH Amsterdam, The Netherlands;* orcid.org/0000-0002-4913-3571

Complete contact information is available at: https://pubs.acs.org/10.1021/acs.jpca.0c03108

Notes

The authors declare no competing financial interest.

■ ACKNOWLEDGMENTS

The authors acknowledge grants of computing time by the Netherlands Scientific Research Council (NWO). This work was carried out under the HPC-EUROPA3 project (project number 730897) with the support of the European Commission Capacities Area, Research Infrastructures Initiative. In particular, M.H. gratefully acknowledges the computer resources and technical support provided by SURFSARA.

■ REFERENCES

(1) Rylander, P. N. *Ulmann's Encyclopedia of Industrial Chemistry*; Wiley-VCH: Weinheim, Germany, 2005.

(2) de Vries, J. G.; Elsevier, C. J. *The Handbook of Homogeneous Hydrogenation*; Wiley-VCH: Weinheim, Germany, 2008.

(3) Samec, J. S. M.; Bäckvall, J.-E.; Andersson, P. G.; Brandt, P. Mechanistic Aspects of Transition Metal-Catalyzed Hydrogen Transfer Reactions. *Chem. Soc. Rev.* **2006**, *35*, 237−248.

(4) Welch, G. C.; Juan, R. R. S.; Masuda, J. D.; Stephan, D. W. Metal-Free Hydrogen Activation. *Science* **2006**, *314*, 1124−1126.

(5) Welch, G. C.; Stephan, D. W. Facile Heterolytic Cleavage of Dihydrogen by Phosphines and Boranes. *J. Am. Chem. Soc.* **2007**, *129*, 1880−1881.

(6) Ullrich, M.; Lough, A. J.; Stephan, D. W. Reversible, Metal-Free, Heterolytic Activation of H_2 at Room Temperature. *J. Am. Chem. Soc.* **2009**, *131*, 52−53.

(7) Hounjet, L. J.; Bannwarth, C.; Garon, C. N.; Caputo, C. B.; Grimme, S.; Stephan, D. W. Combinations of Ethers and B(C6F5)3 Function as Hydrogenation Catalysts. *Angew. Chem., Int. Ed.* **2013**, *52*, 7492−7495.

(8) Mahdi, T.; Stephan, D. W. Enabling Catalytic Ketone Hydrogenation by Frustrated Lewis Pairs. *J. Am. Chem. Soc.* **2014**, *136*, 15809−15812.

(9) Scott, D. J.; Fuchter, M. J.; Ashley, A. E. Nonmetal Catalyzed Hydrogenation of Carbonyl Compounds. *J. Am. Chem. Soc.* **2014**, *136*, 15813−15816.

(10) Stephan, D. W. Frustrated Lewis Pairs. *J. Am. Chem. Soc.* **2015**, *137*, 10018−10032.

(11) Stephan, D. W.; Erker, G. Frustrated Lewis Pair Chemistry: Development and Perspective. *Angew. Chem., Int. Ed.* **2015**, *54*, 6400−6441.

(12) Stephan, D. W. The Broadening Reach of Frustrated Lewis Pair Chemistry. *Science* **2016**, *354*, No. aaf7229.

(13) Wang, L.; Daniliuc, G. K.; Brinkkötter, C. G.; Wiegand, M.; Wübker, T.; Eckert, A. L.; Liu, H.; Brandenburg, L.; Grimme, J. G.; Erker, S.; Solid, G. State Frustrated Lewis Pair Chemistry. *Chem. Sci.* **2018**, *9*, 4859−4865.

(14) Liu, L. L.; Cao, L. L.; Zhu, D.; Zhou, J.; Stephan, D. W. Homolytic Cleavage of Peroxide Bonds via a Single Electron Transfer of a Frustrated Lewis Pair. *Chem. Commun.* **2018**, *54*, 7431−7434.

(15) Paradies, J. From Structure to Novel Reactivity in Frustrated Lewis Pairs. *Coord. Chem. Rev.* **2019**, *380*, 170−183.

(16) Heshmat, M. Alternative Pathway of CO2 Hydrogenation by Lewis-Pair-Functionalized UiO-66 MOF Revealed by Metadynamics Simulations. *J. Phys. Chem. C* **2020**, *124*, 10951−10960.

(17) Rokob, T. A.; Hamza, A.; Stirling, A.; Soós, T.; Pápai, I. Turning Frustration into Bond Activation: A Theoretical Mechanistic Study on Heterolytic Hydrogen Splitting by Frustrated Lewis Pairs. *Angew. Chem., Int. Ed.* **2008**, *47*, 2435−2438.

(18) Rokob, T. A.; Hamza, A.; Stirling, A.; Pápai, I. On the Mechanism of B(C6F5)3-Catalyzed Direct Hydrogenation of Imines: Inherent and Thermally Induced Frustration. *J. Am. Chem. Soc.* **2009**, *131*, 2029−2036.

(19) Rokob, T. A.; Hamza, A.; Pápai, I. Rationalizing the Reactivity of Frustrated Lewis Pairs: Thermodynamics of H2 Activation and the Role of Acid-Base Properties. *J. Am. Chem. Soc.* **2009**, *131*, 10701−10710.

(20) Hamza, A.; Stirling, A.; Rokob, T. A.; Pápai, I. Mechanism of Hydrogen Activation by Frustrated Lewis Pairs: A Molecular Orbital Approach. *Int. J. Quantum Chem.* **2009**, *109*, 2416−2425.

(21) Grimme, S.; Kruse, H.; Goerigk, L.; Erker, G. The Mechanism of Dihydrogen Activation by Frustrated Lewis Pairs Revisited. *Angew. Chem., Int. Ed.* **2010**, *49*, 1402−1405.

(22) Durfey, B. L.; Gilbert, T. M. Computational Studies of Lewis Acidities of Tris(fluorophenyl)-Substituted Boranes: An Additive Relationship Between Lewis Acidity and Fluorine Position. *Inorg. Chem.* **2011**, *50*, 7871.

(23) Ashley, A. E.; Herrington, T. J.; Wildgoose, G. G.; Zaher, H.; Thompson, A. L.; Rees, N. H.; Kramer, T.; O'Hare, D. Separating Electrophilicity and Lewis Acidity: The Synthesis, Characterization, and Electrochemistry of the Electron Deficient Tris(aryl)boranes $B(C_6F_5)n$ (C_6Cl_5) (n = 1 - 3). *J. Am. Chem. Soc.* **2011**, *133*, 14727−14740.

(24) Rokob, T. A.; Bakó, I.; Stirling, A.; Hamza, A.; Pápai, I. Reactivity Models of Hydrogen Activation by Frustrated Lewis Pairs: Synergistic Electron Transfers or Polarization by Electric Field. *J. Am. Chem. Soc.* **2013**, *135*, 4425−4437.

(25) Skara, G.; Pinter, B.; Top, J.; Geerlings, P.; Proft, F. D.; Vleeschouwer, F. D. Conceptual Quantum Chemical Analysis of Bonding and Noncovalent Interactions in the Formation of Frustrated Lewis Pairs. *Chem. - Eur. J.* **2015**, *21*, 5510−5519.

(26) Bistoni, G.; Auer, A. A.; Neese, F. Understanding the Role of Dispersion in Frustrated Lewis Pairs and Classical Lewis Adducts: A Domain-Based Local Pair Natural Orbital Coupled Cluster Study. *Chem. - Eur. J.* **2017**, *23*, 865−873.

(27) Dorkó, É.; Kotai, B.; s Foldes, T.; Gyormore, A.; Pápai, I.; Soos, T. Correlating Electronic and Catalytic Properties of Frustrated Lewis Pairs for Imine Hydrogenation. *J. Organomet. Chem.* **2017**, *847*, 258−262.

(28) Skara, G.; Vleeschouwer, F. D.; Geerlings, P.; Proft, F. D.; Pinter, B. Heterolytic Splitting of Molecular Hydrogen by Frustrated and Classical Lewis Pairs: A Unified Reactivity Concept. *Sci. Rep.* **2017**, *7*, No. 16024.
(29) Wu, D.; Liu, A.; Jia, D. Density Functional Reactivity Theory Characterizing the Reactivity of Frustrated Lewis Pairs. *Comput. Theor. Chem.* **2018**, *1131*, 33−39.
(30) Liu, L.; Lukose, B.; Jaque, P.; Ensing, B. Reaction Mechanism of Hydrogen Activation by Frustrated Lewis Pairs. *Green Energy Environ.* **2018**, *4*, 20−28.
(31) Pu, M.; Privalov, T. How Frustrated Lewis Acid/Base Systems Pass through Transition-State Regions: H_2 Cleavage by [tBu3P/B(C6F5)3]. *Chem. Phys. Chem.* **2014**, *15*, 2936−2944.
(32) Liu, L.; Lukose, B.; Ensing, B. Hydrogen Activation by Frustrated Lewis Pairs Revisited by Metadynamics Simulations. *J. Phys. Chem. C* **2017**, *121*, 2046−2051.
(33) Liu, L.; Lukose, B.; Ensing, B. A Free Energy Landscape of CO2 Capture by Frustrated Lewis Pairs. *ACS Catal.* **2018**, *8*, 3376−3381.
(34) Daru, J.; Bako, I.; Stirling, A.; Pápai, I. Mechanism of Heterolytic Hydrogen Splitting by Frustrated Lewis Pairs: Comparison of Static and Dynamic Models. *ACS Catal.* **2019**, *9*, 6049−6057.
(35) Houghton, A. Y.; Autrey, T. Calorimetric Study of the Activation of Hydrogen by Tris(pentafluorophenyl)borane and Trimesitylphosphine. *J. Phys. Chem. A* **2017**, *121*, 8785−8790.
(36) Scott, D. J.; Fuchter, M. J.; Ashley, A. E. Metal-Free Hydrogenation Catalyzed by an Air-Stable Borane: Use of Solvent as a Frustrated Lewis Base. *Angew. Chem., Int. Ed.* **2014**, *53*, 10218−10222.
(37) Mahdi, T.; Stephan, D. W. Facile Protocol for Catalytic Frustrated Lewis Pair Hydrogenation and Reductive Deoxygenation of Ketones and Aldehydes. *Angew. Chem., Int. Ed.* **2015**, *54*, 8511−8514.
(38) Gyömöre, Á.; Bakos, M.; Földes, T.; Pápai, I.; Domján, A.; Soos, T. Moisture-Tolerant Frustrated Lewis Pair Catalyst for Hydrogenation of Aldehydes and Ketones. *ACS Catal.* **2015**, *5*, 5366−5372.
(39) Das, S.; Pati, S. K. On the Mechanism of Frustrated Lewis Pair Catalysed Hydrogenation of Carbonyl Compounds. *Chem. - Eur. J.* **2017**, *23*, 1078−1085.
(40) Piers, W. E. The Chemistry of Perfluoroaryl Boranes. *Adv. Organomet. Chem.* **2004**, *52*, 1−76.
(41) Hill, P. J.; Herrington, T. J.; Rees, N. H.; Whitea, A. J. P.; Ashley, A. E. H_2 Activation by a Highly Electron-Deficient Aralkylated Organoborane. *Dalton Trans.* **2015**, *44*, 8984−8992.
(42) Blagg, R. J.; Simmons, T. R.; Hatton, G. R.; Courtney, J. M.; Bennett, E. L.; Lawrence, E. J.; Wildgoose, G. G. Novel B(Ar')2(Ar″) Hetero-Tri(aryl)boranes: a Systematic Study of Lewis Acidity. *Dalton Trans.* **2016**, *45*, 6032−6043.
(43) Körte, L. A.; Schwabedissen, J.; Soffner, M.; Blomeyer, S.; Reuter, C. G.; Vishnevskiy, Y. V.; Neumann, B.; Stammler, H. G.; Mitzel, N. W. Tris(perfluorotolyl)borane-A Boron Lewis Superacid. *Angew. Chem., Int. Ed.* **2017**, *56*, 8578−8582.
(44) Heshmat, M.; Privalov, T. Structurally Flexible Oxocarbenium/Borohydride Ion Pair: Dynamics of Hydride Transfer on the Background of Conformational Roaming. *J. Phys. Chem. A* **2018**, *122*, 5098−5106.
(45) Heshmat, M.; Privalov, T. Surprisingly Flexible Oxonium/Borohydride Ion Pair Configurations. *J. Phys. Chem. A* **2018**, *122*, 3713−3727.
(46) Frisch, M. J.; Trucks, G. W. et al.*Gaussian 16*, Revision A.03; Gaussian Inc.: Wallingford, CT, 2016.
(47) Grimme, S.; Antony, J.; Ehrlich, S.; Krieg, H. A Consistent and Accurate ab initio Parametrization of Density Functional Dispersion Correction (DFT-D) for the 94 Elements H-Pu. *J. Chem. Phys.* **2010**, *132*, 154104−154119.
(48) Grimme, S. Semiempirical GGA-type Density Functional Constructed with a Long-Range Dispersion Correction. *J. Comput. Chem.* **2006**, *27*, 1787−1799.
(49) Heshmat, M.; Privalov, T. A Prediction of Proton-Catalyzed Hydrogenation of Ketones in Lewis Basic Solvent through Facile Splitting of Hydrogen Molecules. *Chem. - Eur. J.* **2017**, *23*, 1036.
(50) Bakó, I.; Stirling, A.; Bálint, S.; Pápai, I. Association of Frustrated Phosphine-Borane Pairs in Toluene: Molecular Dynamics Simulations. *Dalton Trans.* **2012**, *41*, 9023−9025.
(51) Pu, M.; Privalov, T. Ab Initio Dynamics Trajectory Study of the Heterolytic Cleavage of H_2 by a Lewis Acid $[B(C_6F_5)_3]$ and a Lewis Base $[P(tBu)_3]$. *J. Chem. Phys.* **2013**, *138*, 154305−115412.
(52) Grimme, S. Exploration of Chemical Compound, Conformer, and Reaction Space with Meta-Dynamics Simulations Based on Tight-Binding Quantum Chemical Calculations. *J. Chem. Theory Comput.* **2019**, *155*, 2847−2862.
(53) Pracht, P.; Bohle, F.; Grimme, S. Automated Exploration of the Low-energy Chemical Space with fast Quantum Chemical Methods. *Phys. Chem. Chem. Phys.* **2020**, *22*, 7169−7192.
(54) Heshmat, M.; Privalov, T. H_2 Cleavage by Frustrated Lewis Pairs Characterized by the Energy Decomposition Analysis of Transition States: An Alternative to the Electron Transfer and Electric Field Models. *J. Phys. Chem. A* **2018**, *122*, 7202−7211.
(55) te Velde, G.; Bickelhaupt, F. M.; Baerends, E. J.; Guerra, C. F.; van Gisbergen, S. J. A.; Snijders, J. G.; Ziegler, T. Chemistry with ADF. *J. Comput. Chem.* **2001**, *22*, 931−967.
(56) Baerends, E. J.; Ziegler, T. et al.*ADF 2019*, Theoretical Chemistry; Vrije Universiteit Amsterdam: The Netherlands, 2019.
(57) Schirmer, B.; Grimme, S. Quantum Chemistry of FLPs and Their Activation of Small Molecules: Methodological Aspects. *Top Curr. Chem.* **2013**, *332*, 213−230.
(58) Heshmat, M.; Privalov, T. Water and a Borohydride/Hydronium Intermediate in the Borane-Catalyzed Hydrogenation of Carbonyl Compounds with H2 in Wet Ether: A Computational Study. *J. Phys. Chem. B* **2018**, *122*, 8952−8962.

https://dx.doi.org/10.1021/acs.jpca.0c03108
J. Phys. Chem. A 2020, 124, 6399−6410